Optimizing Transmission and Propulsion Powers for Flying Base Stations

Mohammadsaleh Nikooroo, Zdenek Becvar
Department of Telecommunication Engineering, Faculty of Electrical Engineering
Czech Technical University in Prague
Prague, Czech Republic
nikoomoh@fel.cvut.cz, zdenek.becvar@fel.cvut.cz

***Abstract*—Unmanned aerial vehicles acting as flying base stations (FlyBSs) have been considered as an efficient tool to enhance capacity of mobile networks and to facilitate communication in emergency cases. The enhancement provided by such network necessitates a dynamic positioning of the FlyBSs with respect to the users. Despite that, the power consumption of the FlyBS remains an important issue to be addressed due to limitations on the capacity of FlyBS's batteries. In this paper, we propose a novel solution combining a transmission power control and the positioning of the FlyBS in order to ensure quality of service to the users while minimizing total consumed power of the FlyBS. We derive a closed-form solution for joint transmission and propulsion power optimization in a single future step. Moreover, we also provide a numerical method to solve the joint propulsion and transmission power optimization problem when a realistic (i.e. inaccurate) prediction of the users' movement is available. According to the simulations, the proposed scheme brings up to 26% of total FlyBS's power saving compared to existing solutions.**

***Index Terms*—Flying base station, transmission power, propulsion power, prediction, mobile users, mobile networks, 6G**

I. Introduction

Deployment of Flying Base Stations (FlyBSs) is a promising technique to address multiple concerns in wireless networks. In contrast to the conventional static base stations, the FlyBSs feature exclusive advantages due their high-mobility, which enables to adapt the network topology to an environment and actual user requirements on communication. This makes FlyBSs a suitable solution for various applications including surveillance in an area [1], offloading traffic from static base stations (BSs) [2], emergency operations [3], extending coverage [4]-[7], collection of data from IoT devices [8],[9], or improving quality of service for users [10]-[12]. In [13], several key challenges regarding the FlyBS's services to the users are listed. These challenges include, among others, positioning of the FlyBSs to provide coverage for as many users as possible, controlling the FlyBSs' power consumption to enhance their serving duration, or maximizing the quality of service (e.g., throughput). The problem of maximizing the coverage for networks with single FlyBS is studied in [4] and [6]. The authors in [7] investigate optimization of the number of required FlyBSs to guarantee the service quality to all ground users in a given area. The authors in [14] adopt evolutionary-based algorithms to maximize the users' satisfaction in terms of experienced data rates. In [10], the authors study the problem of the uplink throughput maximization in a scenario with multiple-antenna FlyBS. However, in all these papers, the power consumption is not addressed at all.

The problem of power consumption in a network with a fixed-wing FlyBS along with the ground users is investigated in [15]. The objective is to identify the trajectory of the FlyBS along several ground users and collect/deliver information from/to these users while minimizing the total power spent by the FlyBSs for flying and communication. Then, in [16], the same problem for rotary-wing FlyBS is studied. In [17], a reinforcement-learning (RL) framework is proposed to control the power consumption in the mobile networks with multiple FlyBSs. However, in [15], [16], and [17], the impact of transmission power is ignored and only the propulsion power spent for the movement of the FlyBS is considered. The efficient 3D placement of the FlyBSs with the consideration of transmission power minimization is studied in several works with a variety of goals including maximization of the number of covered users [18], maximization of the downlink coverage [5], maximization of network throughput [19], maximization of the users' quality-of-experience (QoE) [20], etc. These works are focused on reducing the FlyBSs' transmission power, but the power consumption due to the movement of the FlyBS is not considered. The energy consumption caused by the FlyBS's movement as well as by transmission of data is considered in [21]. However, the work is focused on a scenario in which the FlyBS tracks a mobile target. In such scenario, the constraint on quality of communication towards the users is ignored.

In our previous work [22], the combination of both the FlyBS's transmission power and propulsion power is considered for a single-point optimization. The single-point optimization is understood as adjustment of the FlyBS position and transmission power between each two time steps of the FlyBS

This work was supported by Grant No. P102-18-27023S funded by Czech Science Foundation and by the grant of Czech Technical University in Prague No. SGS17/184/OHK3/3T/13

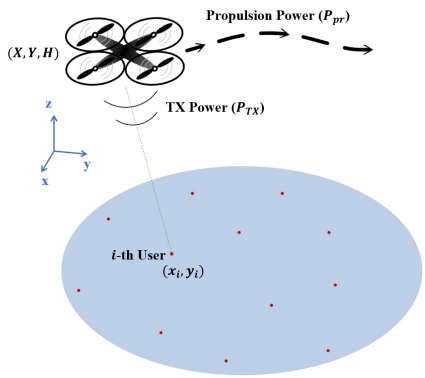

Fig. 1. System model with multiple mobile users deployed within coverage area of the FlyBS.

operation disregarding potential (even inaccurate) estimation of future movement of the users that could further reduce the total power consumption. Moreover, the model proposed in [22] assumes the propulsion power as a linear function of the FlyBS's velocity, which might not be realistic for rotary-wing FlyBSs as shown in [16].

In this paper, we analytically express the total power consumption as a function of the users' relative location with respect to the FlyBS and users requirements on the downlink capacity. Then a closed-form solution is provided for the case of single-point optimization, where, similar to [22], the total power is minimized between two consecutive time steps, although here we adopt a realistic non-linear model for the propulsion power consumption of the rotary-wing FlyBSs, which makes the solution significantly more complicated. Furthermore, a numerical solution is proposed to reduce the total power consumption over multiple time steps (multi-point optimization), as the idea of single-point optimization does not show a good performance in scenarios where the movement velocity of the ground users is very high. We show the performance of the proposed solution and compare it to the existing approaches. Our proposed method shows up to 26% improvement in the total power consumption compared with state-of-the-art methods.

The rest of the paper is organized as follow. In section II, we present the system model. The problem of the power optimization via determination of the FlyBS position and transmission power is presented in Section III. In section IV, we provide simulation results and compare performance with existing solutions. Last section concludes the paper and outlines potential directions to the future research.

II. System Model and Formulations

We consider a mobile network cell with a rotary-wing FlyBS that serves n mobile users in an area as shown in Fig. 1. All n users in the area communicate directly with the FlyBS.

Let $\{X(t), Y(t), H(t)\}$ denote the location of the FlyBS at the time t. By adopting the model from [15], we assume that the FlyBS operates at a fixed altitude H. Hence, the FlyBS can either hover or flight horizontally over the area. Let $\{x_i(t), y_i(t)\}$ denote the coordinates of the i-th ground user at the time t. Then, $d_i(t)$ denotes Euclidian distance of the i-th user to the FlyBS at time t.

We adopt orthogonal downlink channel allocation for all users as considered in a conventional mobile network. Thus, we assume no interference among channels of different users. With that, the channel capacity of the i-th user is calculated from the Shannon–Hartley theorem as:

$$C_i(t) = B_i \log_2(1 + \frac{p_i^R(t)}{N_i}), \tag{1}$$

where B_i denotes the bandwidth of the i-th user's channel, N_i denotes the noise power at the channel of the i-th user, and $p_i^R(t)$ is the received power by the i-th user at time t.

According to the Friis transmission equation, the transmission power of the FlyBS to the i-th user (p_i^T) is given as:

$$p_i^T = Q_i d_i^2, \tag{2}$$
$$Q_i = \frac{p_i^R (4\pi f_c)^2}{G_i^T G_i^R c^2},$$

where G_i^T is the gain of the FlyBS's antenna, G_i^R is the gain of the user's antenna, f_c is the communication frequency, and $c = 3 \times 10^8$m/s is the speed of light. Note that the coefficient $\frac{p_i^R (4\pi f_c)^2}{G_i^T G_i^R c^2}$ is denoted by Q_i for the ease of presentation in later discussions. Note that we assume the antennas of all users with the same gain. From (2), we can conclude that the power consumed by the FlyBS due to transmission power P_{TX} is expressed as a function of the coordinates of the users and the FlyBS as follow:

$$P_{TX}(X, Y, H, t_k) = \sum_{i=1}^{n} Q_i d_i^2 = \tag{3}$$
$$\sum_{i=1}^{n} Q_i ((X(k) - x_i(k))^2 + (Y(k) - y_i(k))^2 + H^2).$$

Following (3), the average transmission power (denoted as P_{TX}^{avg}) over the time span of $\{t_1, \ldots, t_T\}$ can be written as:

$$P_{TX}^{avg}(t_1, \ldots, t_T) = \frac{1}{T} \sum_{k=1}^{T} \sum_{i=1}^{n} Q_i d_i^2 =$$
$$\frac{1}{T} \sum_{k=1}^{T} \sum_{i=1}^{n} Q_i ((X(k) - x_i(k))^2 + (Y(k) - y_i(k))^2 + H^2). \tag{4}$$

As in many related works, we assume that the current positions of the users are known to the FlyBS (see, e.g. [4], [23], [24]). Also, the FlyBS can determine its own position as the knowledge of the FlyBS's position is needed for a common flying and navigation of the FlyBSs ([25]).

In order to formulate the power spent for the FlyBS's movement (propulsion power), we refer to the model provided in [16] for rotary-wing FlyBSs. In particular, the propulsion power is written as a function of the FlyBS's average velocity (denoted by V) in the following way:

$$P_{pr}(V) = L_0 (1 + \frac{3V^2}{U_{\text{tip}}^2}) + L_i (\sqrt{1 + \frac{V^4}{4v_{0,h}^4}} - \frac{V^2}{2v_{0,h}^2})^{\frac{1}{2}} + \frac{1}{2} d_0 \rho s_r A V^3. \tag{5}$$

where L_0 and L_i are the blade profile and induced powers in hovering status, respectively, U_{tip} denotes the tip speed of the rotor blade, $v_{0,h}$ denotes the mean rotor induced velocity during hovering, d_0 is the fuselage drag ratio, s_r is the rotor solidity, ρ is the air density, and A is the rotor disc area, see [16] for more details about the model.

Note that the FlyBS's average velocity can be calculated by dividing the distance moved between two points with the duration of the movement. In particular, if the FlyBS moves from $\{X(k), Y(k), H\}$ to the new location $\{X(k+1), Y(k+1), H\}$, the average velocity is rewritten as:

$$V(k,k+1) = \frac{1}{\Delta t_k}\sqrt{((X(k+1)-X(k))^2 + (Y(k+1)-Y(k))^2)}, \tag{6}$$

where $\Delta t_k = t_{k+1} - t_k$.

Let us define the initial position of the FlyBS as $(X(0), Y(0), H)$, the average propulsion power over the time period of $\{t_0, \ldots, t_T\}$ is written as:

$$P_{pr}^{avg} = \frac{1}{T}\sum_{k=0}^{T-1} P_{pr}(V(k,k+1)). \tag{7}$$

In order to formulate the total power consumption, we jointly optimize both the communication power and the propulsion power. We consider also the power consumption of on-board circuits at the FlyBS (denoted by $P_{circuit}$). Hence, the average overall power consumption P_{tot}^{avg} is written as:

$$P_{tot}^{avg}(X, Y, H, t_1, \ldots, t_T) = P_{circuit}^{avg} + P_{TX}^{avg} + P_{pr}^{avg} \tag{8}$$

According (3), (4), and (7)), we rewrite P_{tot}^{avg} as:

$$P_{tot}^{avg} = P_{circuit}^{avg} + \frac{1}{T}\sum_{k=1}^{T}\sum_{i=1}^{n} Q_i((X(k)-x_i(k))^2 + (Y(k)-y_i(k))^2 + H^2) + \frac{1}{T}\sum_{k=0}^{T-1} P_{pr}(V(k,k+1)). \tag{9}$$

Equation (9) can be further expanded by using (5) and (6), but we do not show the expanded form to avoid cluttering. Note that $P_{circuit}$ in (8) depends on the FlyBS's computational (processing) and communication chipsets and it can be regarded as a constant [16].

In [26], it is shown that, in order to achieve the optimal network's capacity while neglecting the propulsion power of FlyBS, the optimal coordinates $X_{opt}(k)$ and $Y_{opt}(k)$ of the FlyBS correspond to the center of gravity of the users' positions:

$$\begin{aligned} X_{opt}(k) &= \frac{\sum_{i=1}^{n} Q_i x_i(k)}{\sum_{i=1}^{n} Q_i}, \\ Y_{opt}(k) &= \frac{\sum_{i=1}^{n} Q_i y_i(k)}{\sum_{i=1}^{n} Q_i}. \end{aligned} \tag{10}$$

With a similar logic, in case that the users' capacities are not degraded, (8) indicates the position of the FlyBS that achieves the minimum transmission power. Note that the received power by the users is already incorporated in Q_i $(1 \leq i \leq n)$ according to (2), and so in case the users have different throughputs, the coefficients Q_i are not necessarily equal for different users.

III. Power Optimization and FlyBS Positioning

In this section, we first define the optimization problem. Then, we derive a closed-form solution to the defined problem for case $T = 1$, which is the single-point optimization as in [22], however, with non-linear power consumption model based on [16], which completely changes the solution. Next, we provide a numerical solution for the multi-point optimization problem ($T > 1$), as deriving a closed-form solution for this case is too difficult if not impossible.

A. Problem formulation

We formulate the problem of the total power consumption minimization over the time period T as follow:

$$\begin{aligned} &\underset{X(k),Y(k),H(k)}{\operatorname{argmin}} \quad P_{tot}^{avg}, (1 \leq k \leq T) \\ &s.t. \quad C_j(t) \geq {C_j}^{min}, j \in \{1, ..., n\}, \forall t. \end{aligned} \tag{11}$$

The constraint in (11) guarantees that every user within the coverage area receives the minimum required capacity (denoted by $C_j^{min}, j \in 1, \ldots, n$) at all time. In our case, we define C_j^{min} as the capacity that would be experienced by the j-th user over the duration of $\{t_1, \ldots, t_T\}$ if a static BS was deployed. We remark that the transmission power (and so the total power consumption) is increasing with the received capacity according to (1) and (2). Thus, the minimum total power consumption in (11) occurs when every user receives exactly the minimum required capacity, hence, the constraint can be rewritten as $C_j(t) = C_j^{min} (\forall j \in \{1, \ldots, n\}, \forall t)$. From (1), it is concluded that for a constant capacity, the received power is also constant, which implies that the coefficients Q_i are constants. Hence, the transmission power for each user changes only when there is a relative displacement between the FlyBS and the users (e.g., due to users' movement). Here we note that the optimization problem in (11) is repeated every T time steps to calculate the optimum locations of the FlyBS over time.

B. Closed-form solution for single-point optimization

In this subsection, we derive closed-form solution to the optimization problem when $T = 1$. First, we find the critical points at which the partial derivatives of P_{tot}^{avg} are equal to zero. However, due to the complicated expression of $P_{pr}(V)$ in (5), calculation of the exact closed-form solution is not feasible. More specifically, we find that solving $\frac{\partial P_{tot}^{avg}}{\partial X} = 0$ and $\frac{\partial P_{tot}^{avg}}{\partial Y} = 0$ together leads to calculating the roots of polynomials of degree fourteen, which cannot be provided with algebraic solution. Instead, we find an approximation of $P_{pr}(V)$ using polynomial fitting and then solve $\frac{\partial P_{tot}^{avg}}{\partial X} = 0$ and $\frac{\partial P_{tot}^{avg}}{\partial Y} = 0$ by referring to the approximated expression. More specifically, it is observed that the propulsion power in (5) can be well approximated by a polynomial of degree five with respect to V. Fig. 2 shows the actual and the approximated curves for the FlyBS with physical specifications of the FlyBS provided in [27] for " DJI Spreading Wings S900" (see Table I in [27]). Since the error is negligible, we use the approximated propulsion power (denoted by $P_{pr}^{apx}(V)$) that is expressed as:

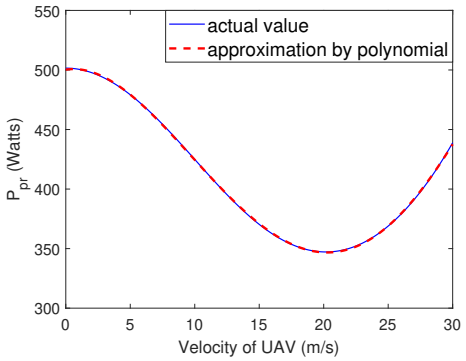

Fig. 2. Actual propulsion power and polynomial approximation vs. velocity of rotary-wing FlyBS.

$$P_{pr}^{apx}(V) = \sum_{j=0}^{5} c_j V^j, \tag{12}$$

$$c_0 = 500.2700, c_1 = 1.6360, c_2 = -1.4103, c_3 = 0.0479,$$
$$c_4 = 2.3521 \times 10^{-4}, c_5 = -1.3452 \times 10^{-5}.$$

The coefficients in (12) are calculated using MATLAB to fit the polynomial to the actual curve with the minimized mean-square-error (MSE).

Now by using P_{pr}^{apx} in (12) and rewriting the equations $\frac{\partial P_{tot}^{avg}}{\partial X} = 0$ and $\frac{\partial P_{tot}^{avg}}{\partial Y} = 0$ for the period of $\{t_0, t_1\}$ we get:

$$\sum_{i=1}^{n} 2Q_i(X(1) - x_i(1)) =$$
$$-\left(\frac{X(1) - X(0)}{\sqrt{(X(1) - X(0))^2 + (Y(1) - Y(0))^2}} \cdot \frac{dP_{pr}^{apx}}{dV}|_{V=V(0,1)}\right.$$

$$\sum_{i=1}^{n} 2Q_i(Y(1) - y_i(1)) =$$
$$-\left(\frac{Y(1) - Y(0)}{\sqrt{(X(1) - X(0))^2 + (Y(1) - Y(0))^2}} \cdot \frac{dP_{pr}^{apx}}{dV}|_{V=V(0,1)}\right. \tag{13}$$

From (13) we derive a new equation as follows

$$\frac{\sum_{i=1}^{n} 2Q_i(X(1) - x_i(1))}{\sum_{i=1}^{n} 2Q_i(Y(1) - y_i(1))} = \frac{X(1) - X(0)}{Y(1) - Y(0)}. \tag{14}$$

Equation (14) can be further rewritten as

$$\frac{(\sum_{i=1}^{n} 2Q_i)X(1) - (\sum_{i=1}^{n} 2Q_i x_i(1))}{(\sum_{i=1}^{n} 2Q_i)Y(1) - (\sum_{i=1}^{n} 2Q_i y_i(1))} = \frac{X(1) - X(0)}{Y(1) - Y(0)}. \tag{15}$$

From (15), it is concluded that (intermediate steps leading to (16) are not presented here):

$$(Y(1) - Y(0)) =$$
$$\frac{(\sum_{i=1}^{n} 2Q_i)Y(0) - (\sum_{i=1}^{n} 2Q_i y_i(1))}{(\sum_{i=1}^{n} 2Q_i)X(0) - (\sum_{i=1}^{n} 2Q_i x_i(1))}(X(1) - X(0)). \tag{16}$$

With (16), we can simplify the expression for V in (6) to

$$V = M|X(1) - X(0)|,$$
$$M = \frac{1}{\Delta t_k}\left(1 + \frac{(\sum_{i=1}^{n} 2Q_i)Y(0) - (\sum_{i=1}^{n} 2Q_i y_i(1))}{(\sum_{i=1}^{n} 2Q_i)X(0) - (\sum_{i=1}^{n} 2Q_i x_i(1))}\right)^{\frac{1}{2}}. \tag{17}$$

Now by expanding the first equation in (13) using (12) and (17) we get:

$$(\sum_{i=1}^{n} 2Q_i)X(1) - (\sum_{i=1}^{n} 2Q_i x_i(1)) = \tag{18}$$
$$-\left(\frac{X(1) - X(0)}{M|X(1) - X(0)|}\right)(5c_5V^4 + 4c_4V^3 + 3c_3V^2 + 2c_2V + c_1) =$$
$$-\left(\frac{X(1) - X(0)}{M|X(1) - X(0)|}\right)(5c_5M^4|X(1) - X(0)|^4 +$$
$$4c_4M^3|X(1) - X(0)|^3 + 3c_3M^2|X(1) - X(0)|^2 +$$
$$2c_2M|X(1) - X(0)| + c_1).$$

Equation (18) can be solved by considering two different possibilities: a) $X(1) > X_0$ (equivalently, $|X(1) - X(0)| = (X(1) - X(0))$ or b) $X(1) < X_0$ (equivalently, $|X(1) - X(0)| = -(X(1) - X(0))$. Presuming a) or b), (18) is rewritten as a quartic function with respect to $X(1)$ that can be provided with a closed-form solution as elaborated below. For $X(1) > X(0)$, (18) is rewritten as:

$$a_4X^4(1) + a_3X^3(1) + a_2X^2(1) + a_1X(1) + a_0 = 0,$$
$$a_4 = 5c_5M^3, \quad a_3 = -20c_5M^3X(0) + 4c_4M^2,$$
$$a_2 = 30c_5M^3X^2(0) - 12c_4M^2X(0) + 3c_3M,$$
$$a_1 = \sum_{i=1}^{n} 2Q_i - 20c_5M^3X^3(0) + 12c_4M^2X^2(0) - 6c_3MX(0) + 2c_2,$$
$$a_0 = 5c_5M^3X^4(0) - 4c_4M^2X^3(0) + 3c_3MX^2(0) - 2c_2X(0) +$$
$$\frac{c_1}{M} - (\sum_{i=1}^{n} 2Q_i x_i(1)). \tag{19}$$

There are four solutions to (19) that are given by:

$$\frac{-a_3}{4a_4} - S \pm \frac{1}{2}\sqrt{-4S^2 - 2p + \frac{q}{S}},$$
$$\frac{-a_3}{4a_4} + S \pm \frac{1}{2}\sqrt{-4S^2 - 2p - \frac{q}{S}}, \tag{20}$$

where

$$p = \frac{8a_4a_2 - 3a_3^2}{8a_4^2}, \quad q = \frac{a_3^3 - 4a_4a_3a_2 + 8a_4^2a_1}{8a_4^3},$$
$$S = \frac{1}{2}\sqrt{\frac{-2}{3}p + \frac{1}{3a_4}(G + \frac{\Delta_0}{G})}, \quad G = \sqrt[3]{\frac{\Delta_1 + \sqrt{\Delta_1^2 - 4\Delta_0^3}}{2}},$$
$$\Delta_0 = a_2^2 - 3a_3a_1 + 12a_4a_0,$$
$$\Delta_1 = 2a_2^3 - 9a_3a_2a_1 + 27a_3^2a_0 + 27a_4a_1^2 - 72a_4a_2a_0. \tag{21}$$

For $X(1) < X_0$, (18) is rewritten as:

$$b_4X^4(1) + b_3X^3(1) + b_2X^2(1) + b_1X(1) + b_0 = 0,$$
$$b_4 = 5c_5M^3, \quad b_3 = -20c_5M^3X(0) - 4c_4M^2,$$
$$b_2 = 30c_5M^3X^2(0) - 12c_4M^2X(0) + 3c_3M,$$
$$b_1 = -\sum_{i=1}^{n} 2Q_i - 20c_5M^3X^3(0) - 12c_4M^2X^2(0) - 6c_3MX(0) - 2c_2,$$
$$b_0 = 5c_5M^3X^4(0) + 4c_4M^2X^3(0) +$$
$$3c_3MX^2(0) + 2c_2X(0) + \frac{c_1}{M} + (\sum_{i=1}^{n} 2Q_i x_i(1)). \tag{22}$$

Similar to (19), there are four solutions to (22) that can be derived by using the coefficients $b_4, ..., b_0$ instead of $a_4, ..., a_0$, respectively. Of course, only the real roots of the quartic functions in (19) and (22) are considered. Furthermore, the solutions to (19) and (22) must meet their presumptive conditions $X(1) > X(0)$ and $X(1) < X(0)$, respectively.

For each of the candidates for $X(1)$, the corresponding value of $Y(1)$ is calculated from (18). In addition to the derived solutions, we also note that $(X(1), Y(1)) = (X(0), Y(0))$ is another critical point of P_{tot}^{avg} (of type 2). By collecting all the (real-valued) critical points, the optimal location of the FlyBS at t_1 (i.e.,$(X(1), Y(1), H)$) can be decided by evaluating P_{tot}^{avg} over $\{t_0, t_1\}$ for all those candidate points for $X(1)$. Next, the optimization is performed over $\{t_1, t_2\}$ to find $(X(2), Y(2), H)$, and so on.

C. Numerical solution for FlyBS power optimization ($T > 1$)

Note that solving the problem (11) requires determination of $2T$ unknown variables in (10), namely $X(k)$ and $Y(k)$ for $1 \leq k \leq T$, and so it is very difficult if not impossible to derive a closed-form expression in general. Instead, we try to optimize P_{tot}^{avg} in (11) by providing a numerical solution. There are several known methods that are commonly used to perform function optimization, such as descent algorithms (Newton's method, Broyden's method, etc.), evolutionary algorithms (genetic algorithms, simulated annealing, etc.), and pattern search methods (Simplex, multidirectional search, etc). The descent algorithms are typically fast in convergence, however, compared to other numerical solvers, they are more likely to get stuck in local optima or even in minimax points. In contrast, the pattern search methods are more reliable to find the global optima of the objective function. Hence, in this paper, we adopt pattern search methods to solve our defined problem. More specifically, we exploit Downhill Simplex Algorithm (also known as Nelder-Mead Algorithm [28]) to find the minimum value of the objective function f (namely, P_{tot}^{avg} in our formulation). This method is based on direct search in multidimensional space (with dimension m) and function comparison using simplex, which is a polytope of $m+1$ vertices in m dimensions. In our setup, each vertex is an m-dimensional point with $m = 2T$ which is corresponding to the (X, Y) sequence of the FlyBS over T time steps. The simplex is updated during following steps:

1. We start from $m+1$ points $P_1, P_2, \ldots, P_{m+1}$. Without loss of generality, we rearrange their indices to satisfy the following order (here we use the general notation of f as the objective function for the sake of simplicity of presentation):

$$f(P_1) \leq f(P_2) \leq \ldots \leq f(P_{m+1}). \tag{23}$$

2. Compute the centroid of all points except P_{m+1}, and let P_0 denote it.

3. Compute the reflected point with reflection coefficient α as:

$$P_r = P_0 + \alpha(P_0 - P_{m+1}). \tag{24}$$

4. If $f(P_1) \leq f(P_r) \leq f(P_m)$, then the simplex is updated by replacing P_{m+1} with P_r, and then we go back to step 1.

5. If $f(P_r) \leq f(P_1)$, the expanded point with expansion coefficient β is calculated as:

$$P_e = P_0 + \beta(P_r - P_0). \tag{25}$$

6. If $f(P_e) \leq f(P_r)$, then the simplex is updated by replacing P_{m+1} with P_e, and going to step 1. Otherwise, we replace P_{m+1} with P_r and then go to step 1.

7. Compute the contracted point with contraction coefficient γ as:

$$P_c = P_0 + \gamma(P_{m+1} - P_0). \tag{26}$$

8. If $f(P_c) \leq f(P_{m+1})$, then we replace P_{m+1} with P_c and go back to step 1. Otherwise, we compute the following shrunk points with shrinkage coefficient δ:

$$P_i = P_1 + \delta(P_i - P_1), 1 \leq i \leq m+1, \tag{27}$$

and then go to step 1.

The termination in this method occurs when the standard deviation of the function values at the simplex vertices falls below a given threshold. It is notable that the performance of Simplex method in terms of precision and termination time relies significantly on the parameters specified in the algorithm, such as the starting point (initial simplex), reflection, expansion, contraction and shrinkage coefficients that should be tuned according to the objective function. We derive the appropriate values of such parameters via experiments. For the initial simplex, we choose the values in the vicinity of the optimal solution. To do this, we use the points derived from the closed-form solution for single-point optimization as elaborated in the previous subsection. We also remark that during the calculation of the initial simplex from the closed form solution, the predicted location of the users are adopted as the reference. The details about the prediction of the users' locations as well as the specifications of Simplex method are elaborated in the next section.

IV. Simulation Results

In this section, we provide details of simulations and models adopted to evaluate the performance of the proposed power control for minimizing the total power consumed by the FlyBS. We also demonstrate the advantages of the proposed scheme over the existing non-optimal scheme.

TABLE I
Parameter Configurations

System Parameter	Numerical value
Number of users in the coverage area, n	180
Antenna gains, G_i^T,G_i^R	0 dBi [33]
Noise power spectral density, N_i	-174 dBm/Hz
Minimum capacity for the j-th user, C_j^{min}	1 Mbps
Communication frequency, f_c	2.6 GHz
System bandwidth	10 MHz [22]
Simulation step, Δt_j	1 second
Altitude of FlyBS, H	100 meters
Velocity of users, v_i	{2,5,10,12,15,20,25,30}m/s
On-board circuit consumption power, $P_{circuit}$	22 dBm [22]
Simulation Duration	320 seconds
Number of simulation drops	100

A. Simulation scenario and models

The simulations are performed using MATLAB. We consider a scenario where the FlyBS serves users represented by vehicles and/or users in vehicles, for example, during a traffic jam at a road or highway. In such situation, the conventional

network is usually overloaded as plenty of active users are located at a small area with limited network coverage. FlyBS can help to improve communication performance in such a scenario ([26], [29]). More specifically, the users are assumed to move on a 3-lane highway in the positive direction of y-axis. A wide range of velocities of the vehicles is considered ($\{2, 5, 10, 12, 15, 20, 25, 30\}$m/s) to cover different traffic situations. As mentioned in section II, the current positions of the users are assumed to be known to the FlyBS. However, the location of the users at the future time slots are unknown in general. There are many solutions for prediction of the user's movement, see, e.g., [30]-[32]. As each of the users-movement predictions reaches different performance depending on scenario and availability of additional information, the evaluation of our proposal for any specific prediction would lead to validity of the results only for such specific scenario and conditions of the predictor. Thus, we generalize the evaluation across the different predictive models for the position of each user via modeling a general prediction error as follows.

The next position of the users is extrapolated from their last two previous positions and this predicted position is further influenced by an addition of a random error. More specifically, we calculate the expected positions of the users by adding the prediction error to the actual positions of the users as follow:

$$\begin{aligned} x_i(s) &= x_i(0) + e_i^x(s), \\ y_i(s) &= y_i(0) + v_{i,0}^y(s) \times s + e_i^y(s), \end{aligned} \tag{28}$$

where $e_i^x(s)$ and $e_i^y(s)$ denote the added error to the x and y coordinates of the user i at the time s, respectively, and $v_{i,0}^y(s)$ denotes the velocity of the user i in the direction of y-axis at the time s. In our scenario, we consider the following model for $e_i^x(s)$ and $e_i^y(s)$:

$$\begin{aligned} |e_i^x(s)| &\leq W_H, \\ |e_i^y(s)| &\leq \frac{1}{2} v_i^y(s) \times s, \end{aligned} \tag{29}$$

where W_H denotes the highway's width.

Table I shows the values of the system parameters that we adopt in the simulations provided later in this section. For the wireless channel, we assume Free-Space Path Loss (FSPL) model, and omnidirectional antennas with a gain of 0 dBi as considered e.g., in [33]. We set spectral density of noise to be -174 dBm/Hz. The radio frequency $f_c = 2.6$ GHz and a bandwidth of 10 MHz [22] are selected. Following [16], the FlyBS's flight altitude is set to $H = 100$ m. Each simulation is of 320 s duration with a step of 1 s and the results are averaged out over 100 simulation drops (simulation runs).

We investigate four different schemes: i) proposed *multi-point optimization scheme (MPS)* with the location of FlyBS determined by numerical optimization of P_{tot}^{avg} as elaborated in section III; ii) *Single-point optimization scheme (SPS)* as in [22] where the locations of the FlyBS is determined by minimizing P_{tot}^{avg} for $T = 1$, although here we adopt the nonlinear model for propulsion power as in (5); iii) *Minimal TX scheme (MTX)* as studied in [26], where only the transmission power is minimized, and the propulsion power is ignored; iv) *Stationary FlyBS* scheme in which the FlyBS does not move, and so there is no propulsion power consumption.

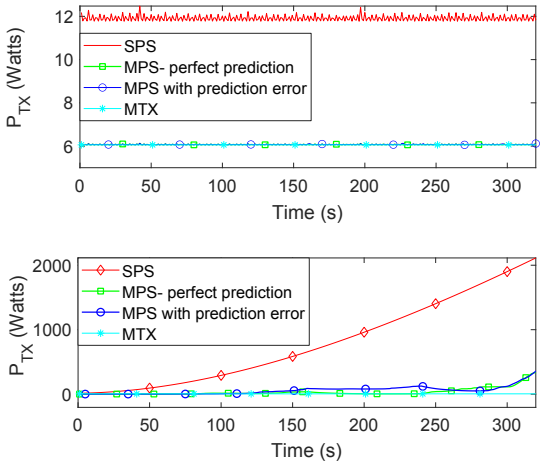

Fig. 3. P_{TX} for different optimization schemes and for $v_i = 5$ m/s (top figure) and 25 m/s (bottom figure).

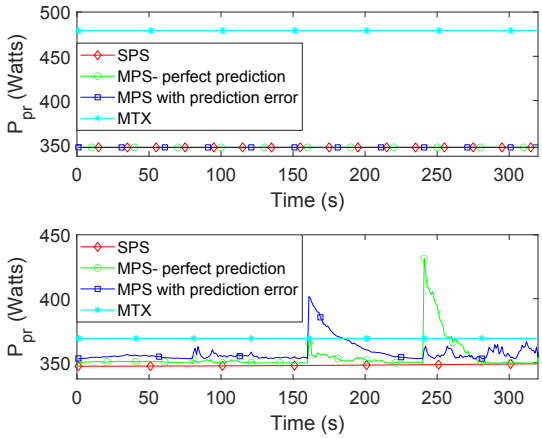

Fig. 4. P_{pr} for different optimization schemes and for $v_i = 5$ m/s (top figure) and 25 m/s (bottom figure).

For the Simplex method we derived the coefficient values for reflection (α), expansion (β), contraction (γ), and shrinkage (δ) factors through experiments as:

$$\alpha = 0.85, \beta = 1.75, \gamma = 0.4, \delta = 0.45. \tag{30}$$

The parameters' values in (30) are selected with respect to the accuracy and the termination time of the method.

B. Simulation results and discussion

First, we compare the average total power between multi-point and single-point optimization schemes.

Figures 3, 4, and 5 illustrate the transmission, propulsion, and total power consumption, respectively, over time for different methods. The figures show the average results for $v_i = 5$ m/s and $v_i = 25$ m/s. For MPS scheme, the duration of optimization period is $T = 80$.

It is observed that at a low velocity of the users, there is no significant change in transmission and propulsion power for

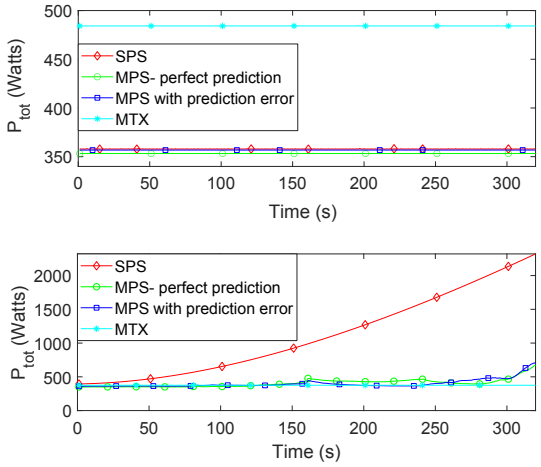

Fig. 5. P_{tot} for different optimization schemes and for $v_i = 5$ m/s (top figure) and 25 m/s (bottom figure).

both MPS and SPS schemes. This is because the propulsion power is a decreasing function at low velocities according to Fig. 2, and this impels the FlyBS to reduce P_{pr} by moving at higher speed than the users. Roughly speaking, at the early steps of movement, this strategy seems to make the FlyBS overtake the center of gravity of the users' locations, which causes an increase in the transmission power. In order to tackle this issue, the FlyBS moves back to the center of gravity after a few steps with almost the same velocity as before (to keep P_{pr} low as well). This strategy is selected by both MPS and SPS, and so there is no significant difference between the performance of the two methods at low users' velocities. It is notable that for high users' velocities, this strategy does not work, as choosing to fly at a lower speed (to reduce P_{pr}) at the beginning steps causes the FlyBS to fall behind the center of gravity, and so it may require the FlyBS to speed up towards the same direction, which introduces more propulsion power. This explains the degradation in SPS scheme's performance at high users' velocities.

According to Fig. 5, the MPS scheme provides a significantly more control over the total power consumption over time, by increasing the FlyBS's speed during some steps to avoid significant increase in transmission power. Note that For Stationary FlyBS scheme (scheme iv as indicated in the previous subsection), the average transmission powers (and so the average total powers) for $v_i = 5$ m/s and 25 m/s are 700 Watts and 18000 Watts, respectively, which is very larger than the average total power consumption in other schemes.

Next, we investigate an impact of the duration of the optimization period on the average power consumption of the FlyBS. Figures 6, 7, and 8 illustrate the average transmission, propulsion, and total power consumptions, respectively, versus the velocity of the vehicles. The results are shown for the optimization periods of $T = \{20, 50, 80\}$. According to all these figures, the power consumption decreases by performing optimization over larger optimization period for all velocities.

According to Fig. 6, there is negligible difference between

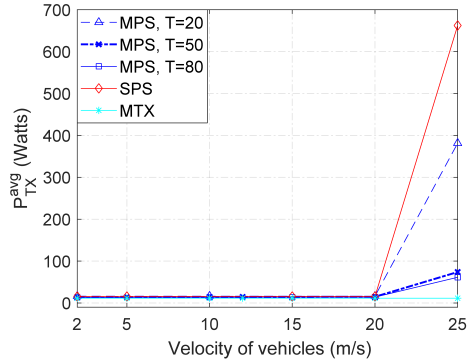

Fig. 6. P_{TX}^{avg} vs. user's velocity for different optimization schemes.

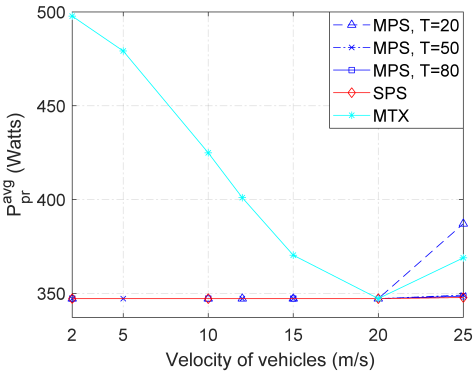

Fig. 7. P_{pr}^{avg} vs. user's velocity for different optimization schemes.

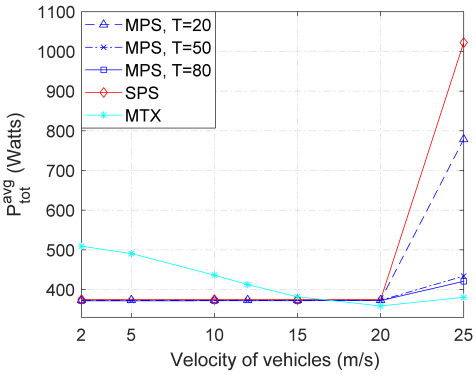

Fig. 8. P_{tot}^{avg} vs. user's velocity for different optimization schemes.

the transmission powers in MPS and SPS schemes for low velocities of the users. As discussed earlier in this section, at low speeds of the users, the FlyBS is basically able to reduce both the transmission and propulsion powers by increasing its speed, and staying close to the center of gravity of the users' locations at the same time. We also explained the reason for significantly increasing behavior of transmission and propulsion powers at high users' speeds. It is observed that the performance gap between MPS and SPS schemes in terms of both propulsion and transmission power is also increasing with respect to velocity, as higher speeds can be interpreted as higher FlyBS's displacements from the center of gravity of the

users, which makes the FlyBS increase either the transmission power or the propulsion power (or both) depending on the values of those powers.

As mentioned before, MTX scheme always ignores the impact of propulsion power. Such strategy causes more propulsion power (and hence more total power) at both high and low speeds where the propulsion cost is higher compared with medium speeds where the propulsion cost is relatively low (which is around the speed of 20 m/s according to Fig. 2). It is also notable that MTX slightly outperforms MPS at very high speeds, although the performance gap is negligible.

Figure 8 shows the advantage of MPS over both SPS and MTX schemes at different speeds. More specifically, the proposed MPS scheme can bring up to 26% improvement in the total power savings compared with MTX in the low-velocity regime, and up to 60% improvement in the total power savings compared with SPS in high-velocity regime.

V. Conclusions

In this paper, we have studied the problem of power optimization in future wireless networks with the FlyBSs. Contrary to existing papers, we optimize the total power consumed by the FlyBS including both the transmission power of the FlyBS and the propulsion power spent for movement of the FlyBS. We first provide closed-form solution determining the position of transmitting power of FlyBS for a realistic non-linear power consumption model in the case of single-point optimization. Then, we develop a numerical solution for the optimal location of the FlyBS and the transmission power of the FlyBS to minimize the total power consumed by the FlyBS over any arbitrary duration (multi-point optimization). We show that the proposed joint transmission power control and FlyBS's movement allows a significant reduction in the total power consumed by the FlyBS while the required capacity of the moving users is always satisfied. In the future, the multiple FlyBS scenario should be studied. In this scenario, association of the users to individual FlyBSs should also be considered.

References

[1] A. Puri, "A survey of unmanned aerial vehicles (UAV) for traffic surveillance," Department of computer science and engineering, University of South Florida, 2005.

[2] J. Lyu, Y. Zeng, and R. Zhang, "UAV-aided offloading for cellular hotspot," *IEEE Trans. Wireless Commun.*, Vol. 17, No. 6, 2018.

[3] K. P. Valavanis and G. J. Vachtsevanos, "Handbook of unmanned aerial vehicles," Springer Publishing Company, Incorporated, 2014.

[4] A. Al-Hourani, S. Kandeepan, and S. Lardner, "Optimal LAP altitude for maximum coverage," *IEEE Commun. Lett.*, Vol. 3, No. 6, 2014.

[5] M. Mozaffari et al., "Efficient deployment of multiple unmanned aerial vehicles for optimal wireless coverage," *IEEE Commun. Lett.*, Vol. 20, No. 8, 2016.

[6] I. Bor-Yaliniz and H. Yanikomeroglu, "The new frontier in ran heterogeneity: Multi-tier drone-cells," *IEEE Communications Magazine*, Vol. 54, No. 11, 2016.

[7] E. Kalantari, H. Yanikomeroglu, and A. Yongacoglu, "On the number and 3D placement of drone base stations in wireless cellular networks," *IEEE VTC Fall*, 2016.

[8] J. Chakareski, "Aerial UAV-IoT sensing for ubiquitous immersive communication and virtual human teleportation," *IEEE INFOCOM Workshops*, 2017.

[9] H. Kim, and J. Ben-Othman, "A collision-free surveillance system using smart UAVs in multi-domain IoT," *IEEE Commun. Lett.*, Vol. 22, No. 12, 2018.

[10] F. Jiang, and A. L. Swindlehurst, "Optimization of UAV heading for the ground-to-air uplink," *IEEE J. Sel. Areas Commun.*, Vol. 30, No. 5, 2012.

[11] V.Sharma, and M. Bennis, "UAV-assisted heterogeneous networks for capacity enhancement," *IEEE Commun. Lett.*, 2016.

[12] L. Wang, "Multiple access mmwave design for UAV-aided 5g communications," *IEEE Wireless Communications*, Vol. 26, 2019.

[13] M. Mozaffari et al., "A tutorial on UAVs for wireless networks: Applications, challenges, and open problems", *IEEE Commun. Surveys Tuts.*, 2019.

[14] J. Plachy et al., "Joint Positioning of Flying Base Stations and Association of Users: Evolutionary-Based Approach," *IEEE Access*, Vol. 7, 2019.

[15] Y. Zeng, and R. Zhang, "Energy-Efficient UAV Communication With Trajectory Optimization," *IEEE Trans. Wireless Commun.*, Vol. 16, No. 6, 2017.

[16] Y. Zeng, J. Xu, and R. Zhang, "Energy Minimization for Wireless Communication With Rotary-Wing UAV," *IEEE Trans. Wireless Commun.*, Vol. 18, No. 4, 2019.

[17] C. Liu et al., "Energy-Efficient UAV Control for Effective and Fair Communication Coverage: A Deep Reinforcement Learning Approach," *IEEE J. Sel. Areas Commun.*, Vol. 36, No. 9, 2018.

[18] H. Shakhatreh et al., "Efficient 3D placement of a UAV using particle swarm optimization," *Proc. IEEE ICICS*, 2017.

[19] Z. Becvar et al., "Positioning of Flying Base Stations to Optimize Throughput and Energy Consumption of Mobile Devices," *IEEE VTC Spring*, 2019.

[20] M. Chen et al., "Caching in the sky: Proactive deployment of cache-enabled unmanned aerial vehicles for optimized quality-of-experience," *IEEE J. Sel. Areas Commun.*, Vol. 35 , No. 5, 2017.

[21] M. Elloumi et al., "Designing an energy efficient UAV tracking algorithm," *IEEE IWCMC*, 2017.

[22] M. Nikooroo, and Z. Becvar, "Joint Positioning of UAV and Power Control for Flying Base Stations in Mobile Networks," *IEEE WiMOB*, 2019.

[23] E. Koyuncu et al., "Deployment and Trajectory Optimization for UAVs: A Quantization Theory Approach," *IEEE WCNC*, 2018.

[24] I. Bor-Yaliniz, A. El-Keyi, and H. Yanikomeroglu, "Efficient 3-D placement of an aerial base station in next generation cellular networks," *IEEE ICC*, 2016.

[25] B. Lee, J. Morrison, and R. Sharma, "Multi-UAV Control Testbed for Persistent UAV Presence: ROS GPS Waypoint Tracking Package and Centralized Task Allocation Capability," *ICUAS*, 2017.

[26] Z. Becvar et al., "Performance of Mobile Networks with UAVs: Can Flying Base Stations Substitute Ultra-Dense Small Cells?," *European Wireless*, 2017.

[27] A. Fotouhi et al., "Survey on UAV Cellular Communications: Practical Aspects, Standardization Advancements, Regulation, and Security Challenges," *IEEE Commun. Surveys Tuts.*, 2019.

[28] J.A. Nelder, and R. Mead, "A simplex method for function minimization," *The Computer Journal*, Vol. 7, No. 4, 1965.

[29] P. Yang et al., "Proactive Drone-Cell Deployment: Overload Relief for a Cellular Network Under Flash Crowd Traffic," *IEEE Trans. Intell. Transp. Syst.*, 2017.

[30] B. Prabhala, and T. La Porta,"Next place predictions based on user mobility traces," *IEEE INFOCOM Workshops*, 2015.

[31] Z. Zhao et al., "A demonstration of mobility prediction as a service in cloudified LTE networks," *IEEE CloudNet*, 2015.

[32] N. Kuruvatti, W. Zhou, and H. Schotten, "Mobility Prediction of Diurnal Users for Enabling Context Aware Resource Allocation," *IEEE VTC Spring*, 2016.

[33] 3GPP Technical Report 36.777, "Technical specification group radio access network; Study on enhanced LTE support for aerial vehicles (Release 15)," 2017.

[34] M. Xiong et al., "A Crowd Simulation Based UAV Control Architecture for Industrial Disaster Evacuation," *IEEE VTC Spring*, 2016.